Location optimisation for antennas by asynchronous particle swarm optimisation

Shu-Han Liao, Chien-Ching Chiu, Min-Hui Ho

Department of Electrical Engineering, Tamkang University, Tamsui District, New Taipei City, Taiwan
E-mail: chiu@ee.tku.edu.tw

Abstract: A novel optimisation procedure for the location of the transmitter in 3×3 multiple input multiple output wireless local area network wireless communication systems is presented. The optimal antenna location for maximising the channel capacity is searched by particle swarm optimiser (PSO) and asynchronous particle swarm optimisation (APSO). There are two different receiver locations considered in the simulation. These two cases are: (i) the transmitter is mobile in the whole indoor environment and the receivers are located on the tables spaced in intervals uniformly distributed (ii) the transmitter is mobile and the receivers are space in uniformly distributed intervals in the whole indoor environment. Numerical results have shown that the proposed PSO and APSO methods are transmit antenna location is optimised to increase channel capacity. The APSO has better optimisation results compared with the PSO and numerical results also show that the APSO outperforms the PSO in convergence speed.

1 Introduction

In recent years, there has been a growing interest in the development of potentially mass-producible application systems using millimetre waves, such as wireless local area networks (WLAN) systems [1, 2]. To develop millimetre-wave WLAN systems, however, we need to know the reflection and transmission characteristics in millimetre-wave bands, so that we can evaluate indoor multipath propagation characteristics and the interactions of millimetre waves with various objects.

This paper addresses basic issues regarding the WLAN systems that operate in the 60 GHz band as part of the fourth-generation system [3]. The 60 GHz band provides 7 GHz of unlicensed spectrum with a potential to develop wireless communication systems with multi-Gbps throughput. The IEEE 802.11 standard committee [4], one of the major organisations in WLAN specifications development, established the IEEE 802.11ad task group to develop an amendment for the 60 GHz WLAN systems.

All wireless systems must be able to deal with the challenges of operating over a multi-path propagation channel, where object in the environment can cause multiple reflections to arrive at the receiver. In general, effective antenna selection and deployment strategies are important for reducing bit error rate (BER) in indoor wireless systems [5, 6]. In general, the transmission quality is estimated with strength of power in the narrowband communication system. In this paper, the best transceiver locations by PSO and asynchronous particle swarm optimisation (APSO) to improve wireless communication system performance in real environment are presented. Based on the channel capacity formula, the channel capacity instead of signal power is chosen as the objective function. Then this location problem is transformed into the optimisation problem. Since this optimisation problem is often highly non-linear and non-differentiable, particle swarm optimiser (PSO) is used to search the transmitter location to maximising the channel capacity of the communication system. Moreover, different values of dielectric constant and conductivity of materials for different frequencies are carefully considered in channel modelling.

The remaining sections of this paper are organised as follows: Section 2 briefly explains the formulation of the problem that includes ultra-wideband (UWB) channel modelling, calculations of channel capacity and descriptions of PSO and APSO. The numerical results are then presented in Section 3 and conclusion is made in Section 4.

2 System description

2.1 Channel modelling

Using ray-tracing [7–24] approaches to predict channel characteristic is effective and fast, and the approaches are also usually applied to multiple input multiple output (MIMO) channel modelling in recent years [25–28]. Thus, a ray-tracing technique is developed to calculate the channel matrix of MIMO system in this paper. A flow chart of the ray-tracing process is shown in Fig. 1. It conceptually assumes that many triangular ray tubes (not rays) are shot from a transmitter. Here the triangular ray tubes whose vertexes are on a sphere are determined by the following method. First, we construct an icosahedron which is made of 20 identical equilateral triangles. Then, each triangle of the icosahedron is tessellated into many smaller equilateral
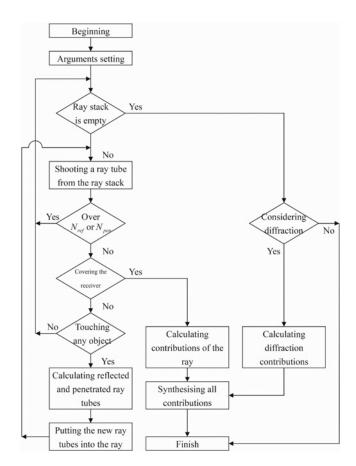
Fig. 1 *Flow chart of the ray-tracing process*

triangles. Finally, these small triangles are projected onto the sphere and each ray tube whose vertexes are determined by the small equilateral triangle [29].

For each ray tube bouncing and penetrating in the environment, we check whether reflection times and penetration times of the ray tube are larger than the numbers of maximum reflection N_{ref} and maximum penetration N_{pen}, respectively. If not, we check whether the receiver falls within the reflected ray tube. If yes, the contribution of the ray tube to the receiver can be attributed to an equivalent source (i.e. image source). In other words, a specular ray going to the receiver exists in this tube and this ray can be thought as launched from an image source. Moreover, the field diffracted from illuminated wedges of the objects in the environment is calculated by uniform theory of diffraction [30]. Note that only single diffraction is considered in this paper, because the contribution of double diffraction is so small in the analysis. We have simulated the case of double diffraction and found that the impact of the second diffraction is negligible.

By using these images and received fields, the channel frequency response can be obtained as following:

$$H(f) = \sum_{p=1}^{N_p} a_p(f) e^{j\theta_p(f)} \qquad (1)$$

where p is the path index, N_p is the number of paths, f is the frequency of sinusoidal wave, $\theta_p(f)$ is the pth phase shift and $a_p(f)$ is the pth receiving magnitude, which depends on the radiation vector of the transmitting and receiving antenna.

Note that the channel frequency response of MIMO systems can be calculated by (1) in the frequency range of the signal.

2.2 System description

The received signal for a time-invariant narrowband system combining with MIMO (MIMO-NB system) is described as follows [31]

$$Y = HX + W \qquad (2)$$

$$H = \begin{bmatrix} h_{11} & h_{12} & h_{13} & \cdots & h_{1N_t} \\ h_{21} & h_{22} & h_{33} & \cdots & h_{2N_t} \\ h_{21} & h_{22} & h_{33} & \cdots & h_{3N_t} \\ \vdots & \vdots & \vdots & \ddots & \vdots \\ h_{N_r1} & h_{N_r2} & h_{N_r3} & \cdots & h_{N_rN_t} \end{bmatrix} \qquad (3)$$

where X, Y and W denote the $N_t \times 1$ transmitted signal vector, the $N_r \times 1$ received signal vector and the $N_r \times 1$ zero mean additive white Gaussian noise vector at a symbol time, respectively, H is the $N_r \times N_t$ channel matrix and h_{ij} is the complex channel gain from the jth transmitting antenna to the ith receiving antenna.

From linear algebra theory, every linear transformation can be represented as a composition of three operations: a rotation operation, a scaling operation and another rotation operation [32]. As a result, the channel matrix H can be expressed by singular value decomposition (SVD) as follows

$$H = UDV* \qquad (4)$$

where U and $V*$ are the $N_r \times N_r$ and $N_t \times N_t$ unitary matrices, D is an $N_r \times N_t$ rectangular matrix whose diagonal elements are non-negative real values and other elements are zero and the symbol $*$ in (4) stands for the conjugate transpose or Hermitian operation.

MIMO is capable of signal processing at the transmitter and receiver to produce the set of received signals with highest overall capacity. A matrix representation of MIMO-NB system is shown in Fig. 2. In this figure, a linear signal processing operation $\hat{V}$ is multiplied by the transmitted signal vector X to produce a new set of signals. The new set of signals is fed further into the MIMO channel. Finally, another linear signal processing operation $\hat{U}$ is multiplied by the incoming signal propagating through the channel. The final output signal vector $\hat{Y}$ is expressed
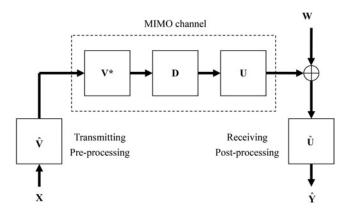

Fig. 2 *Matrix representation of MIMO-NB system*

as follow

$$\hat{Y} = \hat{U}(UDV^*)\hat{V}X + \hat{U}W \qquad (5)$$

Note that there is no adding or subtracting of any signal power in the system, because $\hat{V}$ and $\hat{U}$ are both unitary matrix.

If channel state information (CSI) is known for receiver, the channel capacity of the MIMO-NB system can be written in an equivalent matrix notation for $N_t \geq N_r$ as follows

$$C^{\mathrm{NB}} = B \log_2 \left(\det \left(I + \frac{\mathrm{SNR}_t}{N_t} DD^* \right) \right) \qquad (6)$$

where I is an appropriately sized identity matrix. Using the relationship of $D = U^*HV$, (6) can be rewritten as follows

$$C^{\mathrm{NB}} = B \log_2 \left(\det \left(I + \frac{\mathrm{SNR}_t}{N_t} U^*HH^*U \right) \right) \qquad (7)$$

Since U is an unitary matrix, and it does not change the value of the determinant of the matrix that they multiply. Thus, (7) can be rewritten as follows [33–35]

$$C^{\mathrm{NB}} = B \log_2 \left(\det \left(I + \frac{\mathrm{SNR}_t}{N_t} HH^* \right) \right) \qquad (8)$$

The equation is especially effective to calculate MIMO capacity in a mathematical software package, since the channel capacity needs CSI for the receiver only.

By the ray-tracing technique, all the frequency responses inside the bandwidth of WLAN between any transmitter and receiver antennas are calculated. Then, MIMO channel capacity of WLAN transmission can be calculated as summation of the channel capacity of the narrowband at each discrete frequency point. Thus, the channel capacity (bandwidth efficiency) can be written as

$$C^{\mathrm{WLAN}} = \frac{1}{\mathrm{BW}} \sum_{k=1}^{N_f} C_k^{\mathrm{narrowband}} \quad (\mathrm{bits/s/Hz}) \qquad (9)$$

where BW is the total bandwidth of WLAN and N_f are the numbers of frequency components.

2.3 Evolutionary algorithms

Evolution algorithm starts with an initial population of potential solutions that is composed by a group of randomly generated individuals. Each individual is a D-dimensional vector consisting of D optimisation parameters. The initial population may be expressed by $\{X_j : j = 1, 2, \ldots, Np\}$, where N_p is the population size. The explicit expression for X_j is given in the next section. The details of the PSO and APSO algorithms are given below.

2.3.1 Particle swarm optimisation: In PSO, the particles move in the search space, where each particle position is updated by two optimum positions. The first one is the position (with best fitness) that has been achieved so far for the concerned particle. This position is called $x_{p\mathrm{best}}$. The other one is the global best position obtained so far by any particle in the swarm. This best position is called $x_{g\mathrm{best}}$ [36].

By keeping $x_{p\mathrm{best}}$ and $x_{g\mathrm{best}}$, the update rule for the velocity of each particle is an important mechanism in a PSO algorithm. The most commonly used update rule for the velocity v_j^{k+1} is as follows

$$v_j^{k+1} = \omega \cdot v_j^k + c_1 \cdot \phi_1 \cdot \left(x_{p\mathrm{best}_j}^k - x_j^k \right) + c_2 \cdot \phi_2 \cdot \left(x_{g\mathrm{best}}^k - x_j^k \right)$$
$$(10)$$

$$x_j^{k+1} = x_j^k + v_j^{k+1}, \quad j = 0 \tilde{N}_p - 1 \qquad (11)$$

where c_1 and c_2 are the learning coefficients used to control the impact of the local and global components in velocity (10). v_j^{k+1} and x_j^{k+1} are the velocity and position of the jth particle at generation $k+1$. Both ϕ_1 and ϕ_2 are random numbers with the values uniformly distributed between 0 and 1. ω is a parameter known as the inertia weight.

2.3.2 Asynchronous particle swarm optimisation: Clerc [37] suggested the use of a different velocity update rule, which introduced a parameter ξ called constriction factor. The role of the constriction factor is to ensure convergence when all the particles tend to stop their movement. The flowchart of the APSO algorithm is shown in Fig. 3.

The velocity update rule is then given by

$$v_j^{k+1} = \xi \cdot \left(v_j^k + c_1 \cdot \phi_1 \cdot \left(x_{p\mathrm{best}_j}^k - x_j^k \right) + c_2 \cdot \phi_2 \cdot \left(x_{g\mathrm{best}}^k - x_j^k \right) \right)$$
$$(12)$$

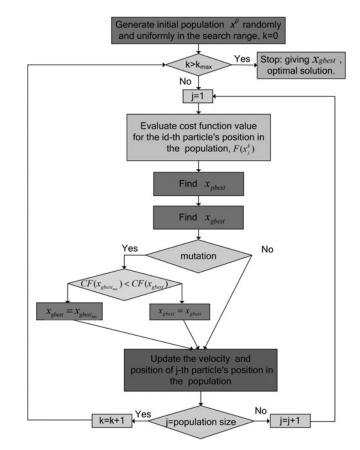$$x_j^{k+1} = x_j^k + v_j^{k+1}, \quad j = 0 \tilde{N}_p - 1 \qquad (13)$$

Fig. 3 *Flow chart for the modified APSO*

where

$$\xi = \frac{2}{\left| 2 - \phi - \sqrt{\phi^2 - 4\phi} \right|}, \quad \phi = c_1 + c_2 \geq 4$$

By (10) and (12), particles fly around in the multidimensional solution space and adjust their positions according to their own experience and the experience of neighbouring particles, by exploiting the knowledge of best positions encountered by themselves and their neighbours [38].

The key distinction between an PSO and the APSO is on the updating mechanism, damping boundary condition and mutation scheme. In the typical synchronous PSO, the algorithm updates all the particles velocities and positions using (10) and (12) at the end of each generation and then updates the best positions, $x_{p\text{best}}$ and $x_{g\text{best}}$. Alternatively, the current updating mechanism of APSO uses the following rule: just after the update by (10) and (12) for each particle the best positions $x_{p\text{best}}$ and $x_{g\text{best}}$ will be replaced if the new position is better than the current best ones such that they can be used immediately for the next particle. In this way, the swarm reacts more quickly to speedup the convergence.

Boundary conditions in PSO play a key role as it is pointed out in [39]. In this paper we have applied the damping boundary condition and mutation scheme. The mutation scheme plays a role in avoiding premature convergences for the searching procedure and helps the $x_{g\text{best}}$ escape from the local optimal position. More details about the APSO algorithm can be found in [40].

2.3.3 Ray-tracing combined optimisation algorithm: By combining the optimisation algorithm and the ray-tracing technique, we are able to optimise antenna location, which can maximise the channel capacity performance.

In the synthesis procedure, the optimisation algorithm is used to minimise the following cost function (CF)

$$\text{CF} = \frac{1}{(1/\text{BW})\sum_{k=1}^{N_f} C_k^{\text{narrowband}}} \tag{14}$$

where CF is the inverse average capacity for UWB system in (9). PSO and APSO are used to search the transmitter antenna location to maximise the capacity of the communication system. Then, the three-dimensional (3D) shooting and bouncing ray (SBR)/image method combined with PSO and APSO has been presented in this paper. In our simulation, when the CF is smaller than the threshold value or PSO and APSO do not find a better individual within 300 successive generations, the PSO and APSO will be terminated and a solution is then obtained.

3 Numerical results

Simulation and numerical results are presented in this section. A ray-tracing technique is developed to calculate the channel frequency response from 59.5 to 60.5 GHz with frequency interval of 5 MHz. That is, 201 frequency components are used. The channel capacities for different transceiver positions in the indoor environment are investigated. Fig. 4 is the top view of the indoor environment with dimensions of 10 m (length) × 9.2 m (width) × 3 m (height). 0.5 m-thick floors and ceilings of the concrete are used for these cases. The transmitting and receiving antenna are modelled with

simple omni-directional radiation pattern and vertically polarisation. Each antenna is of a fixed height of 1 m. The heights of desk, partition and file cabinet are 0.73, 3 and 1.7 m, respectively. The thickness of partition is 0.115 m. Since the same materials for different frequencies will have different propagation characteristics. Therefore the frequency dependence of the dielectric and conductivity of materials are carefully considered in the channel simulation. The frequency response of the indoor environment was calculated by SBR/image method for the 3×3 MIMO-WLAN channel. The number of ray tubes shooting from transmitter is 18 000. The maximum number of bounces setting beforehand is five, and convergence is confirmed. The optimal antenna location for maximising the channel capacity is searched by PSO and APSO.

The values of parameters in PSO and APSO are as follows: population size is set to be 30 in the simulation; selection strategy – constriction coefficient; learning coefficients – $c_1 = 2.8$, $c_2 = 1.3$; probability of mutation − 0.15. These are two cases with different transceiver positions in our simulation. The transmitting antenna $Tx_c(5, 4.6, 1 \text{ m})$ located in the centre of the indoor environment with a fixed height of 1 m is used for our reference, as shown in Fig. 4.

For the first case, the transmitter is mobile in the whole indoor environment and the receivers are located on the tables with uniform intervals distribution, which 120 measurements with 0.5 m spacing between adjacent points are carried out (e.g. transmission from a cell phone to a computer). The optimal locations of the transmitting antennas are at $Tx_{PSO}(2.64, 4.65, 1 \text{ m})$ and $Tx_{APSO}(3.99, 3.76, 1 \text{ m})$ by using PSO and APSO, respectively. The channel capacity against SNR is calculated, as shown in Fig. 5. Here SNR is defined as the ratio of the average transmitted power to noise power at the front end of the receiver. The results show that the capacity curve increases greatly when the Tx_{PSO} and Tx_{APSO} are used as transmitter. Tx_{PSO} and Tx_{APSO} can dramatically increase channel capacity not only because of the beamforming gain and diversity gain but also became MIMO spatial multiplexing technique makes full use of multipath fading. The results
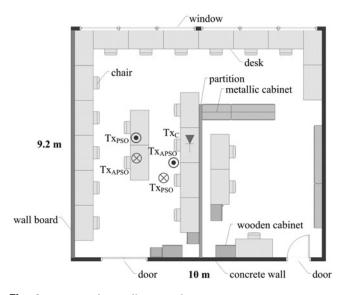

Fig. 4 *Layout of a small personal communication environment.*

◉ denotes the optimal location of the transmitting antenna when the receivers are located on the tables with uniform intervals distribution
⊗ denotes the optimal location of the transmitting antenna when the receivers are with uniform intervals distribution in the whole indoor environment
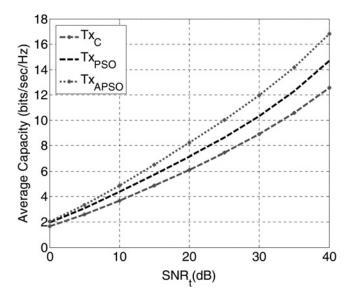
Fig. 5 *Capacity against SNR for the Scenario I*

Fig. 7 *Capacity against SNR for the Scenario II*

show that the capacity curve increases greatly when the Tx_{PSO} and Tx_{APSO} are used as transmitter. It is seen that the channel capacity at SNR = 40 dB is about 12.58, 14.68 and 16.63 for Tx_c, Tx_{PSO} and Tx_{APSO}, respectively. It is clear that channel capacity increased by APSO is better than PSO by about 13.3%. The performance for the antenna location by APSO is much better.

The CFs for against generation PSO and APSO are calculated, as shown in Fig. 6. It is seen that the final CF is reduced by APSO and good convergence is achieved within 172 generations. The CF of APSO is about 0.105 in the final generation. It also shows that the convergent speed for the APSO is faster than that for PSO.

For the second case, the transmitter is mobile and the receivers are spaced in uniformly distribution intervals in the whole indoor environment, when 120 measurements with 0.9 m spacing between adjacent points were carried out (e.g. transmission from one cell phone to the other cell phone). The optimal locations of the transmitting antennas are at Tx_{PSO}(3.72, 3.41, 1 m) and Tx_{APSO}(2.66, 4.23, 1 m) by using the PSO and APSO, respectively. The channel capacity against SNR is calculated, as shown in Fig. 7. The

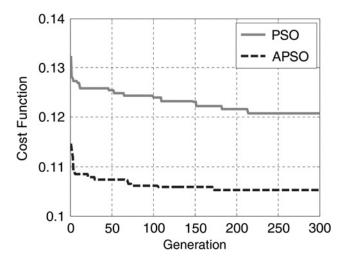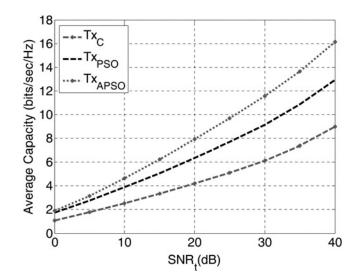results show that the capacity curve increases greatly when using the Tx_{PSO} and Tx_{APSO} as the transmitter. It is seen that the channel capacity at SNR = 40 dB are about 8.97, 12.93 and 16.13 for Tx_c, Tx_{PSO} and Tx_{APSO}, respectively. It is clear that channel capacity increase by APSO is better than PSO by about 24.7%. The performance for the antenna location by APSO is much better.

The CFs for PSO and APSO against generation are calculated, as shown in Fig. 8. It is seen that the final CF is reduced by APSO and good convergence is achieved within 89 generations. The CF of APSO is about 0.123 in the final generation. It also shows that the convergent speed for the APSO is faster than that for PSO.

All of the above results demonstrate that Tx_{PSO} and Tx_{APSO} which is presented in this paper are powerful for two cases of propagation environment. Tx_{PSO} and Tx_{APSO} can dramatically increase channel capacity not only because of the beamforming gain and diversity gain but also became MIMO spatial multiplexing technique makes full use of multipath fading. As a result, the capacity can be increased substantially in indoor UWB communication system.
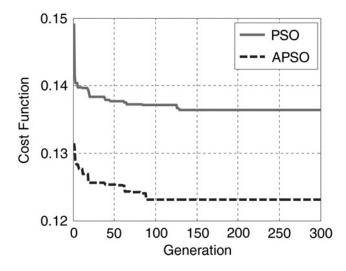

Fig. 6 *Channel capacity average against generation for the Scenario II by PSO and APSO*

Fig. 8 *Channel capacity average against generation for the second case by PSO and APSO*

4 Conclusions

The study has shown that we can deploy transmitter antenna position by PSO and APSO to improve wireless communication system performance in real environment. In this paper, the CF is defined as the inverse of channel capacity for WLAN system. The PSO and APSO minimise the CF by adjusting the transmitter antenna location. Channel propagation environments are simulated the propagation site. To obtain optimal channel capacity for a given transmitter, PSO and APSO algorithms are used to determine the best location of the transmitter. This paper proposes the use of a 3D ray-tracing model in indoor wireless systems, combining PSO and APSO for optimising the transmitter antenna location. It is shown that the combination of the ray-tracing method and the algorithm can lead to optimised channel capacity in indoor environment. By using the frequency responses of these 3×3 MIMO channels, the channel capacity performance for Shannon–Hartley theorem WLAN communication system is calculated. Channel capacity is the average performance criteria for digital transmission systems. The PSO and APSO is used to maximise the channel capacity. The frequency dependence of materials utilised in the structure of the indoor channel is accounted for in the channel simulation, that is, the dielectric constant and loss tangent of obstacles are not assumed to be frequency independent. Numerical results show that the APSO outperforms the PSO in convergence speed. As a result, the channel capacity can be increased by about 24.7% in indoor WLAN communication systems. It is also found that the channel capacity as increased by APSO is better than that by PSO.

5 References

1 Sato, K., Ihara, T., Saito, H., *et al.*: 'Measurements of reflection and transmission characteristics of interior structures of office buildings in the 60 GHz band', *IEEE Trans. Antennas Propag.*, 1997, **45**, (12), pp. 1783–1792
2 Ke, C.H., Wei, C.C., Lin, K.W., Ding, J.W.: 'A smart exponential-threshold-linear backoff mechanism for IEEE 802.11 WLANs.', *Int. J. Commun. Syst.*, 2011, **24**, pp. 1038–1048
3 Smulders, P.: 'Exploiting the 60 GHz band for local wireless multimedia access:prospects and future directions', *IEEE Commun. Mag.*, 2002, **40**, (1), pp. 140–147
4 IEEE Standard for Information Technology – Telecommunications and Information Exchange between Systems – Local and Metropolitan Area Networks – Specific Requirements – Part 11: Wireless LAN Medium Access Control (MAC) and Physical Layer (PHY) Specifications – 2007.IEEE Standard 802.11-2007
5 Wong, A.H., Neve, M.J., Sowerby, K.W.: 'Antenna selection and deployment strategies for indoor wireless communication systems', *IET Commun.*, 2007, **1**, (4), pp. 732–738
6 Lee, D.C.K., Neve, M.J., Sowerby, K.W.: 'The impact of structural shielding on the performance of wireless systems in a single-floor office building', *IEEE Trans. Wirel. Commun.*, 2007, **6**, (5), pp. 1787–1795
7 Liu, C.L., Ho, M.H., Chiu, C.C., Cheng, C.Y.: 'A comparison of UWB communication characteristics for various corridors', *ACTA Int. J. Model. Simul.*, 2010, **30**, (2), pp. 172–177. (EI)
8 Ho, M.H., Chiu, C.C., Liao, S.H.: 'Optimization of channel capacity for MIMO smart antenna using particle swarm optimizer', *IET Commun.*, 2012, **6**, (16), pp. 2645–2563
9 Chiu, C.C., Chen, C.H., Liao, S.H., Chen, K.C.: 'Bit error rate reduction by smart UWB antenna array in indoor wireless communication', *J. Appl. Sci. Eng.*, 2012, **15**, (2), pp. 139–148
10 Ho, M.H., Chiu, C.C., Liao, S.H.: 'Bit error rate reduction for circular ultrawideband antenna by dynamic differential evolution', *Int. J. RF Microw. Comput.-Aided Eng.*, 2012, **22**, (2), pp. 260–271

11 Chiu, C.C., Chen, C.H., Liao, S.H., Tu, T.C.: 'Ultra-wideband outdoor communication characteristics with and without traffic', *EURASIP J. Wirel. Commun. Netw.*, 2012, **92**, pp. 1–14
12 Liao, S.H., Ho, M.H., Chiu, C.C., Lin, C.H.: 'Optimal relay antenna location in indoor environment using particle swarm optimizer and genetic algorithm', *Wirel. Pers. Commun.*, 2012, **62**, (3), pp. 599–615
13 Chiu, C.C., Kao, Y.T., Liao, S.H., Huang, Y.F.: 'UWB communication characteristics for different materials and shapes of the stairs', *J. Commun.*, 2011, **6**, (8), pp. 628–632
14 Liao, S.H., Chen, H.P., Chiu, C.C., Liu, C.L.: 'Channel capacities of indoor MIMO-UWB transmission for different material partitions', *Tamkang J. Sci. Eng.*, 2011, **14**, (1), pp. 49–63
15 Liao, S.H., Ho, M.H., Chiu, C.C.: 'Bit error rate reduction for multiusers by smart UWB antenna array', *Progress Electromagn. Res. C*, 2010, **16. PIER C 16**, pp. 85–98
16 Ho, M.H., Liao, S.H., Chiu, C.C.: 'A novel smart UWB antenna array design by PSO', *Progress Electromagn. Res. C*, 2010, **15. PIER C 15**, pp. 103–115
17 Ho, M.H., Liao, S.H., Chiu, C.C.: 'UWB communication characteristics for different distribution of people and various materials of walls', *Tamkang J. Sci. Eng.*, 2010, **13**, (3), pp. 315–326
18 Liu, C.L., Chiu, C.C., Liao, S.H., Chen, Y.S.: 'Impact of metallic furniture on UWB channel statistical characteristics', *Tamkang J. Sci. Eng.*, 2009, **12**, (3), pp. 271–278
19 Liao, S.H., Chiu, C.C., Ho, M.H.: 'Comparison of dynamic differential evolution and genetic algorithm for MIMO-WLAN transmitter antenna location in indoor environment', *Wirel. Pers. Commun.*, 2013, **71**, (4), pp. 2677–2691
20 Liao, S.H., Chiu, C.C., Chen, C.H., Ho, M.H.: 'Channel characteristics of MIMO-WLAN communications at 60 GHz for various corridors', *EURASIP J. Wirel. Commun. Netw.*, 2013, **96**, pp. 1–10
21 Chiu, C.C., Ho, M.H., Liao, S.H.: 'MIMO-UWB smart antenna communication characteristics for different antenna arrays of transmitters', *Int. J. RF Microw. Comput. -Aided Eng.*, 2013, **23**, (2), pp. 378–392
22 Chiu, C.C., Ho, M.H., Liao, S.H.: 'PSO and APSO for optimizing coverage in indoor UWB communication system', *Int. J. RF Microw. Comput.-Aided Eng.*, 2013, **23**, (3), pp. 300–308
23 Chiu, C.C., Yu, C.Y., Liao, S.H., Wu, M.K.: 'Channel capacity of multiple-input multiple-output systems for optimal antenna spacing by particle swarm optimizer', *Wirel. Pers. Commun.*, 2013, **69**, (4), pp. 1865–1876
24 Ho, M.H., Chiu, C.C., Liao, S.H.: 'Comparison of different antenna arrays for the BER reduction in indoor wireless communication', *Int. J. Commun. Syst.*, 2013, **26**, (2), pp. 161–176
25 Loredo, S., Rodríguez-Alonso, A., Torres, R.P.: 'Indoor MIMO channel modeling by rigorous GO/UTD-based ray tracing', *IEEE Trans. Veh. Technol.*, 2008, **57**, (2), pp. 680–692
26 Malik, W.Q., Stevens, C.J., Edwards, D.J.: 'Spatio-temporal ultra-wideband indoor propagation modeling by reduced complexity geometric optics', *IEET Commun.*, 2007, **1**, (4), pp. 751–759
27 Yu, J.L., Wu, C.H., Lee, M.F.: 'MC-CDMA MIMO systems with quasi-orthogonal space–time block codes: Channel estimation and multiuser detection', *Int. J. Commun. Syst.*, 2012, **25**, pp. 294–313
28 Jiang, D., Zhang, H., Yuan, D.: 'Joint precoding and power allocation for multiuser transmission in MIMO relay networks', *Int. J. Commun. Syst.*, 2012, **25**, pp. 205–220
29 Chen, S.H., Jeng, S.K.: 'An SBR/image approach for radio wave propagation in indoor environments with metallic furniture', *IEEE Trans. Antennas Propag.*, 1997, **45**, (1), pp. 98–106
30 Biglier, E., Calderbank, R., Constantnides, A., Goldsmith, A., Paulraj, A., Poor, H.V.: 'MIMO wireless communications' (Cambridge University Press, New York, 2007)
31 Strang, G.: 'Linear algebra and its applications' (Harcourt Brace Jovanovich, San Diego, 1988)
32 Balanis, C.A.: 'Advanced engineering electromagnetics' (John Wiley & Sons Press, USA, 1989)
33 Xu, Z., Sfar, S., Blum, R.S.: 'Analysis of MIMO systems with receive antenna selection in spatially correlated Rayleigh fading channels', *IEEE Trans. Veh. Technol.*, 2009, **58**, (1), pp. 251–262
34 Chang, W.J., Tarng, J.H., Peng, S.Y.: 'Frequency-space-polarization on UWB MIMO performance for body area network applications', *IEEE Antennas Wirel. Propag. Lett.*, 2008, **7**, pp. 577–580
35 Valenzuela-Valdés, J.F., García-Fernández, M.A., Martínez-González, A.M., Sánchez-Hernández, D.A.: 'The influence of efficiency on receive diversity and MIMO capacity for Rayleigh-fading channels', *IEEE Trans. Antennas Propag.*, 2008, **56**, (5), pp. 1444–1450
36 Kennedy, J., Eberhart, R.C.: 'Particle swarm optimization'. Proc. IEEE Int. Conf. Neural Network, 1995, pp. 1942–1948

37 Clerc, M.: 'The swarm and the queen: towards a deterministic and adaptive particle swarm optimization'. Proc. Congress Evolutionary Computation, Washington, DC, 1999, pp. 1951–1957

38 Donelli, M., Massa, A.: 'Computational approach based on a particle swarm optimizer for microwave imaging of two-dimensional dielectric scatterers', *IEEE Trans. Microw. Theory Tech.*, 2005, **53**, (5), pp. 1761–1776

39 Huang, T., Mohan, A.S.: 'A hybrid boundary condition for robust particle swarm optimization', *IEEE Antennas Wirel. Propag. Lett.*, 2005, **4**, pp. 112–117

40 Rekanos, I.T., Trochidis, A.: 'Shape reconstruction of two-dimensional acoustic obstacle using particle swarm optimization', *Acta Acust. United with Acust.*, 2007, **93**, (6), pp. 917–923